Supporting information

The PspF-binding domain $PspA_{1-144}$ and the PspA·F complex - New insights into the coiled-coil dependent regulation of AAA+ proteins

Osadnik *et al.* (2015)

contains

Supporting Figures S1-S6
Supporting tables S1-S2

Figure S1

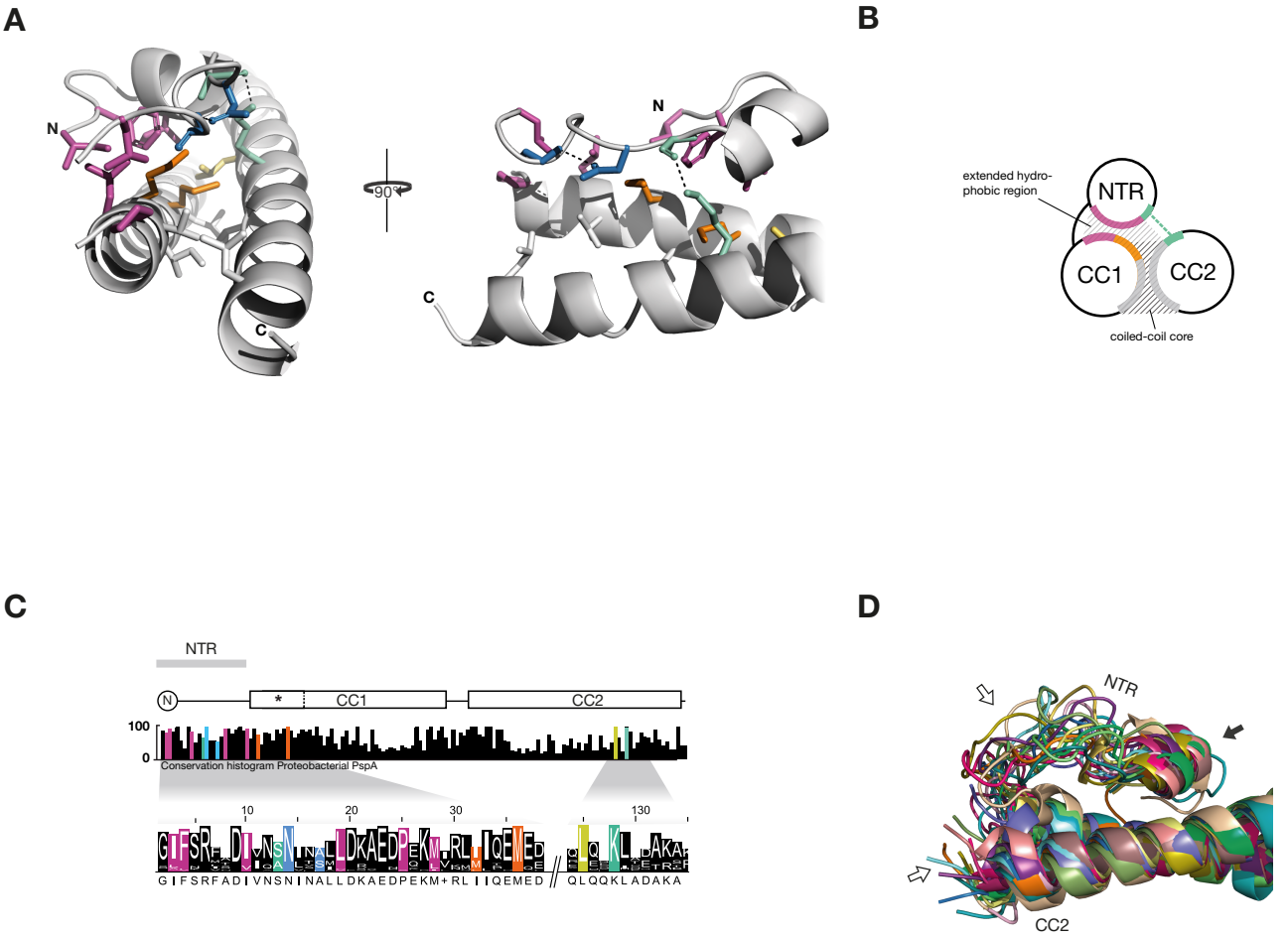
A
N
C
90°
N
C
B
extended hydro-
phobic region
NTR
CC1
CC2
coiled-coil core
C
NTR
N
*
CC1
CC2
100
0
Conservation histogram Proteobacterial PspA
10
20
30
130
G I F S R F A D I V N S N I N A L L D K A E D P E K M + R L I Q E M E D // Q L Q Q K L A D A K A
D
NTR
CC2
E
NTR

Figure S2

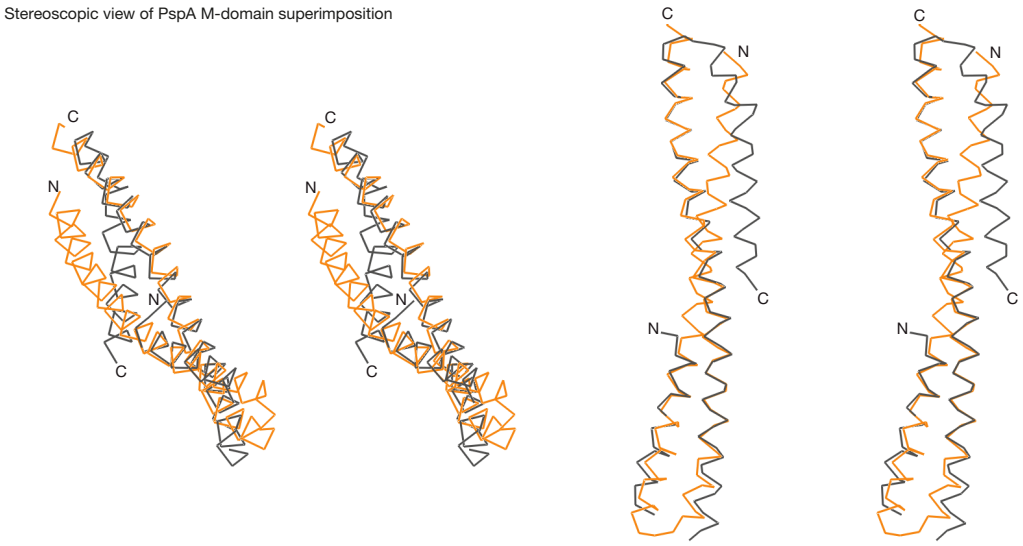
Stereoscopic view of PspA M-domain superimposition
C
N
N
C
C
N
N
C
C
N
N
C
C
N
N
C

Figure S3

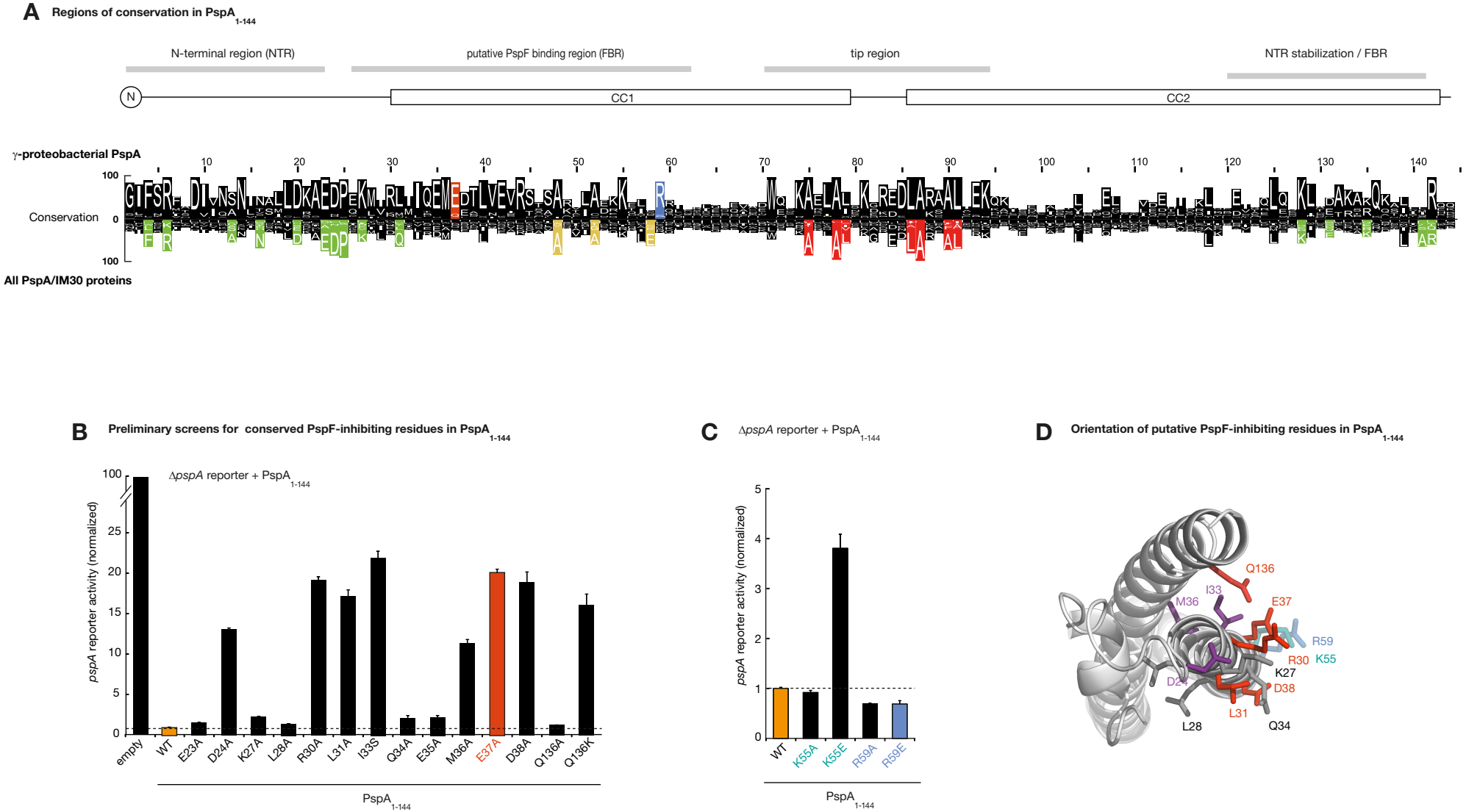
A
Regions of conservation in PspA1-144
N-terminal region (NTR)
putative PspF binding region (FBR)
tip region
NTR stabilization / FBR
N
CC1
CC2
γ-proteobacterial PspA
Conservation
All PspA/IM30 proteins
B
Preliminary screens for conserved PspF-inhibiting residues in PspA1-144
ΔpspA reporter + PspA1-144
pspA reporter activity (normalized)
empty
WT
E23A
D24A
K27A
L28A
R30A
L31A
I33S
Q34A
E35A
M36A
E37A
D38A
Q136A
Q136K
PspA1-144
C
ΔpspA reporter + PspA1-144
pspA reporter activity (normalized)
WT
K55A
K55E
R59A
R59E
PspA1-144
D
Orientation of putative PspF-inhibiting residues in PspA1-144
Q136
I33
M36
E37
R59
R30
K55
K27
D24
D38
L31
L28
Q34

Figure S4

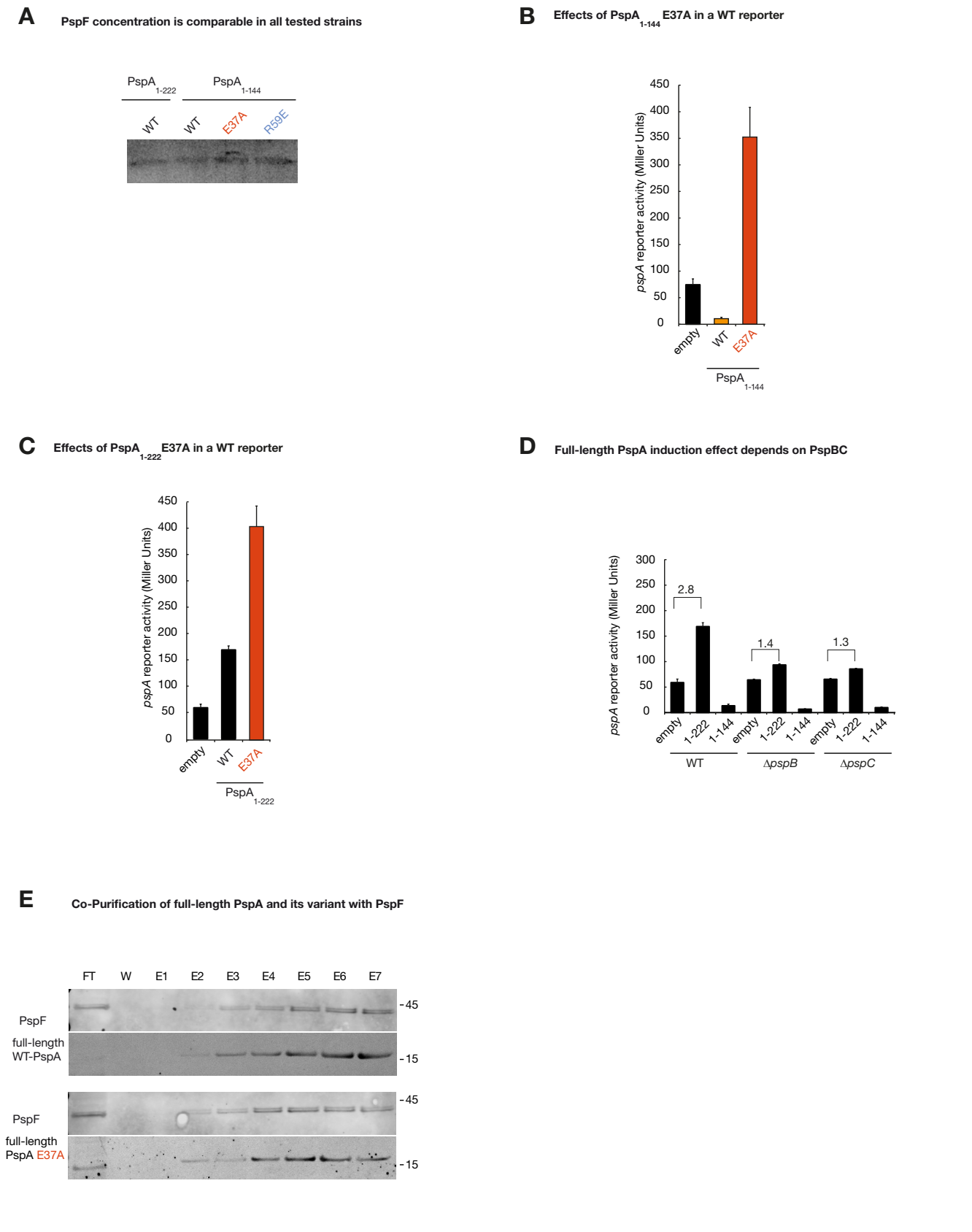
A
PspF concentration is comparable in all tested strains
PspA1-222
PspA1-144
WT
WT
E37A
R59E
B
Effects of PspA1-144 E37A in a WT reporter
pspA reporter activity (Miller Units)
450
400
350
300
250
200
150
100
50
0
empty
WT
E37A
PspA1-144
C
Effects of PspA1-222 E37A in a WT reporter
pspA reporter activity (Miller Units)
empty
WT
E37A
PspA1-222
D
Full-length PspA induction effect depends on PspBC
pspA reporter activity (Miller Units)
300
250
200
150
100
50
0
2.8
1.4
1.3
empty
1-222
1-144
WT
ΔpspB
ΔpspC
E
Co-Purification of full-length PspA and its variant with PspF
FT
W
E1
E2
E3
E4
E5
E6
E7
PspF
full-length WT-PspA
PspF
full-length PspA E37A
45
15
45
15

Figure S5

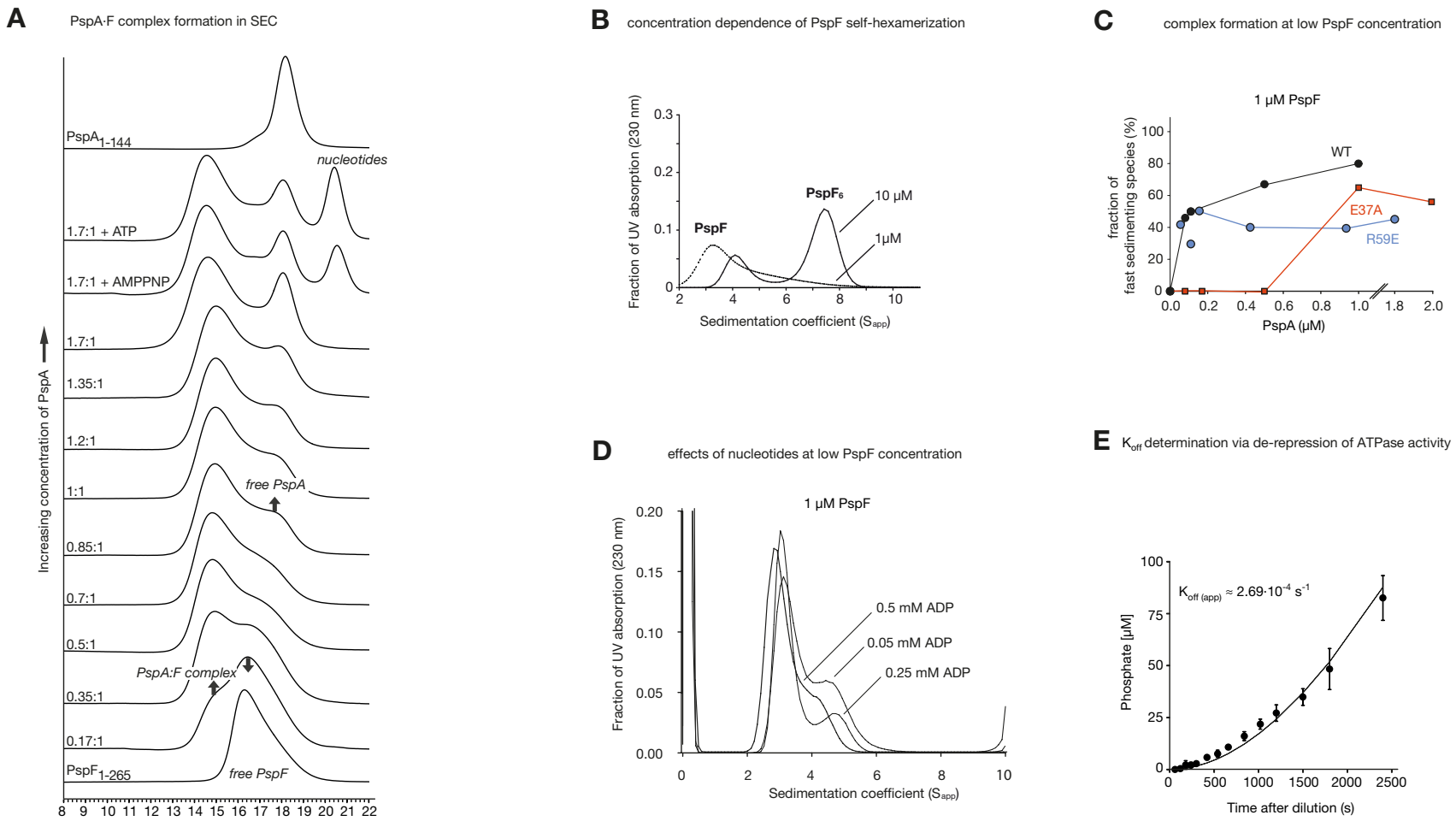
A
PspA·F complex formation in SEC
PspA1-144
nucleotides
1.7:1 + ATP
1.7:1 + AMPPNP
1.7:1
1.35:1
1.2:1
1:1
free PspA
0.85:1
0.7:1
0.5:1
PspA:F complex
0.35:1
0.17:1
PspF1-265
free PspF
Increasing concentration of PspA
8 9 10 11 12 13 14 15 16 17 18 19 20 21 22
B
concentration dependence of PspF self-hexamerization
Fraction of UV absorption (230 nm)
PspF
PspF6
10 µM
1µM
Sedimentation coefficient (Sapp)
C
complex formation at low PspF concentration
1 µM PspF
fraction of fast sedimenting species (%)
WT
E37A
R59E
PspA (µM)
D
effects of nucleotides at low PspF concentration
1 µM PspF
Fraction of UV absorption (230 nm)
0.5 mM ADP
0.05 mM ADP
0.25 mM ADP
Sedimentation coefficient (Sapp)
E
Koff determination via de-repression of ATPase activity
Koff (app) ≈ 2.69·10-4 s-1
Phosphate [µM]
Time after dilution (s)

Figure S6

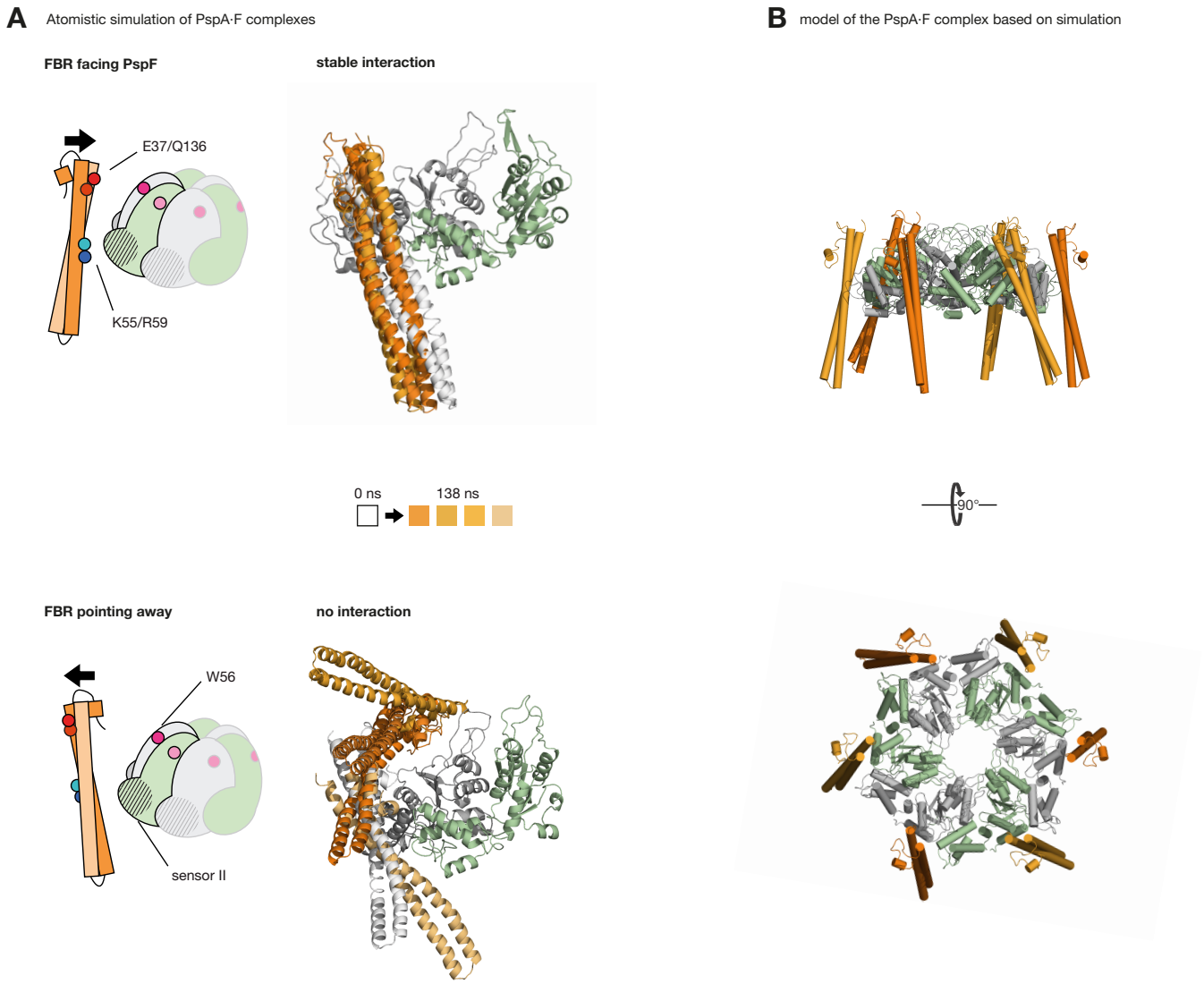
A
Atomistic simulation of PspA·F complexes
FBR facing PspF
stable interaction
E37/Q136
K55/R59
0 ns
138 ns
FBR pointing away
no interaction
W56
sensor II
B
model of the PspA·F complex based on simulation
90°

Supplementary Figure Legends

Figure S1: The N-terminal region folds back to the PspF-binding domain. Important amino acids (in a,b,c): ■ conserved hydrophobic amino acids that attach the NTR to CC1; ■ hydrophobic coiled-coil core forming residues; ■ laterally protruding hydrophobic amino acids from CC1 and one from CC2 (■) that link the hydrophobic core of the coiled coil and the hydrophobic region formed by the back-folding NTR; ■ a residue of CC2 (Lys128) that contacts the NTR; ■ Asn14 and Ala17, whose backbone is contacted by Asn14. Asn14 is needed for PspC interaction, see discussion. **(a)** front and side view of the back-folding N-terminus. **(b)** Schematic depiction of the front view in A, showing the large hydrophobic face of CC1 and the extended hydrophobic region formed by the coiled-coil core and the back-folding NTR (▨). **(c)** Conservation histogram of γ-proteobacterial PspA (overview) and detailed excerpts showing the high overall degree of conservation of the highlighted amino acids. **(d)** The N-terminal region is flexible, but stably attached to CC1 and CC2 during atomistic simulations. $PspA_{1-144}$ molecules (n=19) were aligned in their NTR/CC1 region after 18 ns of simulation (avg.). Even though the rest of the protein as well as the NTR moved considerably and the NTR showed high flexibility in the region 13-24 (⇩), it was still tightly attached to CC1 (⇩). **(e)** The less well defined electron density of the crystal structure in the N-terminal region indicates flexibility of this region as well. *Cartoon* representation of $PspA_{1-144}$, colored according to B-factor of residues in the crystal structure, arrows as in D.

Figure S2: Stereoscopic views of superimposed backbones of ClpB-MD (■) and PspA (■) from the alignment shown in Fig. 3A, as described in the main text.

Figure S3: Preliminary screen to identify putative change of inhibition variants of $PspA_{1\text{-}144}$.

(a) Full overview of regions of $PspA_{1\text{-}144}$ drawn on top of comparative consensus profiles of γ-proteobacterial PspA (upper part) and PspA/IM30-family proteins (lower part) indicating regions of structurally important amino acids (i.e. conserved in both profiles) as well as amino acids putatively important for proteobacterial PspAs only (i.e., not conserved in all PspA/IM30-family proteins). Colors for structurally important amino acids in PspA/IM30 as in Fig.2.

(b, c) Preliminary screen of single amino-acid variants of PspA either in the N-terminal (c) or the C-terminal (c) part of the region conserved in γ-proteobacteria using a long-induction LacZ-activity assay. All data normalized to repression level of the wild-type fragment. Several exchanges show markedly reduced inhibition of PspF compared to the wild-type fragment (■), or, in the case of the R59E variant, slightly increased repression. Variants E37A and R59E were used for detailed studies of PspF inhibition. Even weaker inhibiting variants (up to 25-fold higher *psp* levels) still strongly inhibit PspF, as the empty vector control has a 100-fold increased *psp* level (panel b, *empty*)

(d) Orientation of variants on the PspA structure. Variants from the screen in (b) are colored depending on the strength of their effect (■- surface residues and ■ non-surface residues with strong loss of inhibition; ■ weak to no effect on inhibition). Loss of inhibition variants cluster on one face of PspA and point into the same direction as residues R59 and K55, indicating a putative PspF binding patch, see also Fig.4A.

Figure S4: Effects of PspA variants in PspF regulation *in vivo*

(a) The PspF level in reporter strains with constitutively produced PspF is indeed comparable and not influenced by different variants. Western Blot developed against the strep-tag of PspF-strep after 3h induction (0.1% arabinose), compare to LacZ assays in Fig.4D.

(b) The upregulating effect of $PspA_{1-144}$-E37A also exists in the full *psp* wild-type background and is therefore independent of *pspF* overproduction. Long-term induction (compare to Fig.4D, right) leads to strong induction of *psp*, while the wild-type fragment shows repression of *psp* as before.

(c) The E37A variant has the same up-regulating effect if introduced into full-length PspA ($PspA_{1-222}$), i.e. upregulation of *psp*. Experimental setup as in panel b. Note that this upregulation is much stronger than the general increase of *psp* induction due to PspA overproduction, which we found to be largely dependent on PspBC (see panel d).

(d) PspBC cause most of the inducing effect of long-term PspA overproduction. Comparison of changes in *pspA* reporter levels in the wild-type *psp* background (WT) or *ΔpspB* and *ΔpspC* single gene deletion mutants caused by production of either full-length PspA (1-222) or the fragment used in this study (1-144) in comparison to the empty vector control (empty). The 2.8-fold induction in the wild-type background is reduced to ~1.4-fold reporter levels in both deletion mutants. The only PspF interacting fragment $PspA_{1-144}$ inhibits *psp* in all backgrounds.

(e) Co-elution of strep-tagged PspF with his-tagged full-length PspA-E37A from the reporter strain, with wild-type PspA shown as comparison (cf. Fig.4E)

Figure S5: $PspA_{1-144}$· $PspF_{1-265}$ complex formation.

(a) Size exclusion chromatography with $PspF_{1-265}$ and $PspA_{1-144}$ indicates complex formation. Ratio of PspA relative to PspF is given on the left at the start of each chromatogram. PspA·F appears at very low relative concentrations of PspA (0.17:1), while free PspA only appears at nearly equimolar concentrations. Preincubation with nucleotides (ATP/AMPPNP) and $MgCl_2$ (second and third chromatogram from the top) does not change complex formation.
(b) Influence of $PspF_{1-265}$ concentration on self-hexamerization. Distribution of sedimentation coefficients of 1 or 10 µM PspF and their relative abundance (integrated absorption at 230 nm).
(c) Relative portion of the fast sedimenting species during titration (see Fig.5B) as percentage of total UV-absorption (230 nm) in the sample cuvette. Addition of 0.08 µM $PspA_{1-144}$ already leads to a shift of 46% of $PspF_{1-265}$-absorption (the absorption of PspA is negligible at this point).
(d) Stable oligomerization of $PspF_{1-265}$ in equilibrium is not promoted by ADP. Distribution of sedimentation coefficients of 1 µM PspF with 0.05 to 0.5 mM ADP (≈ 5-fold K_D) and their relative abundance (integrated absorption at 230 nm). Larger concentrations of ADP could not be measured due the high UV-absorption of nucleotides and the low amount of protein. Since $PspF_{1-265}$ shows ATPase-activity *in vitro* at 1 µM, this data does not exclude transient hexamer formation that occurs spontaneously. Still, stable oligomerization of PspF upon addition, which could be shown in the case of PspA (cf. Fig.5B), is not observed.
(e) Determination of the apparent dissociation constant (k_{off}) of the PspA·F complex. Jump dilution (1:40) of the concentrated $PspA_{1-144}$· $PspF_{1-265}$ complex into the ATPase assay. The k_{off} was determined (Tummino & Copeland, 2008) via curve fitting, with the hydrolysis rate of an equilibrated sample serving as reference rate.

Figure S6: Atomistic simulations of complex stability of PspA and PspF. **(a)** Four independent atomistic simulations of $PspA_{1-144}$ and $PspF_{1-275}$ after 138 ns of simulated time (starting position of PspA was the same for all of them, shown in white cartoon representation, results of the four simulations in shades of orange superimposed on the right). Stable complex formation occurred when the FBR was facing PspF (schematically depicted on the left). In contrast, PspA diffuses away during simulation when PspA is rotated 180° around its longitudinal axis so that the FBR points away from PspF initially. In the superimposed pictures of simulations on the right, all PspFs were omitted for clarity but the two from the starting conditions, since PspF did not unfold or change its structure considerably during simulations.

(b) The modeled $PspA_{1-144} \cdot PspF_{1-265}$ complex based on the stable binding conformation shown in panel b.

Supplemental Table S1. Primers used in this study.

cloning of pspA$_{1-144}$	
pspA-F	CCATGGGTATTTTTTCTCGCTTTGC
pspA144-R	CTCGAGCTGATGACGTAACATCAATGC
single amino acid exchanges	
pspA-ex-E23A	CTGTTAGAGAAAGCGGCTGATCCACAGAAACTGG / CCAGTTTCTGTGGATCAGCCGCTTTCTCTAACAG
pspA-ex-D24A	GAGAAAGCGGAAGCTCCACAGAAACTGG / CCAGTTTCTGTGGAGCTTCCGCTTTCTC
pspA-ex-L28A	GGAAGATCCACAGAAAGCGGTTCGTCTGATGATC / GATCATCAGACGAACCGCTTTCTGTGGATCTTCC
pspA-ex-L31A	CAGAAACTGGTTCGTGCGATGATCCAGGAGATG / CATCTCCTGGATCATCGCACGAACCAGTTTCTG
pspA-ex-Q34A	CTGGTTCGTCTGATGATCGCAGAGATGGAAGATACACTG / CAGTGTATCTTCCATCTCTGCGATCATCAGACGAACCAG
pspA-ex-E37A	GATGATCCAGGAGATGGCAGATACACTGGTTGAAG / CTTCAACCAGTGTATCTGCCATCTCCTGGATCATC
pspA-ex-K55A	CGTTGGCAGAAAAGGCACAGCTGACTCGC / GCGAGTCAGCTGTGCCTTTTCTGCCAACG
pspA-ex-K55E	CGTTGGCAGAAAAGGAACAGCTGACTCG / CGAGTCAGCTGTTCCTTTTCTGCCAACG
pspA-ex-R59A	GAAAAGAAACAGCTGACTGCCCGTATTGAACAAGCGTC / GACGCTTGTTCAATACGGGCAGTCAGCTGTTTCTTTTC
pspA-ex-R59E	GAAAAGAAACAGCTGACTGAACGTATTGAACAAGCGTCGG / CCGACGCTTGTTCAATACGTTCAGTCAGCTGTTTCTTTTC
pspA-ex-Q136A	CACGCGCTCGCGCCCAGGCATTGATGTTACGTCATCAGTGACTCGAGATATA / TATATCTCGAGTCACTGATGACGTAACATCAATGCCTGGGCGCGAGCGCGTG
pspA-ex-Q136K	CACGCGCTCGCAAACAGGCATTGATGTTACGTCATCAGTGACTCGAGATATA / TATATCTCGAGTCACTGATGACGTAACATCAATGCCTGTTTGCGAGCGCGTG
BspHI-dependent mutagenesis	
pspA-BspHI-L31-F[1]	TCATGATTCAGGAGATGGAAGATACAC
pspA-BspHI-L31-R[1]	TCATGAGACGAACCAGTTTCTGTG
pspA-BspHI-R30A	TCATGAGTGCAACCAGTTTCTGTGGATCTTC
pspA-BspHI-I33S	TCATGAGCCAGGAGATGGAAGATACAC
pspA-BspHI-E35A	TCATGATTCAGGCAATGGAAGATACACTGGTTGAAG
pspA-BspHI-M36A	TCATGATTCAGGAGGCAGAAGATACACTGGTTGAAGTACG
pspA-BspHI-D38A	TCATGATTCAGGAGATGGAAGCAACACTGGTTGAAGTACGTTCTAC
cloning of pspF	
pspF-F[2]	CATATGGCAGAATACAAAGATAATTTACTTGGT
pspF265-R[2]	GGATCCGGCGATAGCGTCTTCAG
pspF-R[3]	AAGCTTACTCGAGAATCTGGTGCTTTTTCAACAACG

Primer sequences are given in 5'-3' direction. [1]Primers used for introduction of a BspHI site at the position that codes for Leu31 in the amino acid sequence. [2]Restriction sites at the 5' end of the primer are omitted for clarity (NdeI for pspF-F, BamHI for pspF265-R). [3] Reverse primer (5' HindIII site) for cloning of *pspF* into pUL-P_{tat} contains a XhoI site before the HindIII site for future introduction of tags

Supplemental Table S2. Data collection and refinement statistics.

Dataset	PspA1-144 native	Se-PspA1-144 MAD remote	Se-PspA1-144 MAD peak	Se-PspA1-144 MAD inflection
Radiation source	BESSY BL14.1	BESSY BL 14.1	BESSY BL 14.1	BESSY BL14.1
Wavelength (Å)	0.9184	0.9759	0.9798	0.9799
Energy (kEV)	13.5000	12.7100	12.6540	12.6525
Resolution range (Å)	39.73 - 1.8	39.80 - 2.01	39.87 - 2.01	39.87 - 2.06
Highest resolution shell (Å)	1.9 - 1.8	2.13 - 2.01	2.13 - 2.01	2.18 - 2.06
Space group	C2	C2	C2	C2
Cell dimensions				
a, *b*, *c* (Å)	79.65, 30.38, 80.48	79.72, 30.39, 80.70	79.95, 30.47, 80.87	79.94, 30.43, 80.94
α, β, γ (°)	90, 115.61, 90	90, 115.27, 90	90, 115.29, 90	90, 115.28, 90
R_{merge}	3.1 (39.8)	5.2 (40.9)	4.7 (42.7)	4.8 (40.4)
$I / \sigma I$	20.5 (3.5)	11.0 (2.0)	11.7 (1.9)	12.0 (2.0)
Completeness (%)	96.8 (95.6)	96.8 (94.8)	96.7 (95.1)	96.8 (95.8)
Multiplicity	3.4 (3.4)	2.2 (2.2)	2.2 (2.20)	2.2 (2.2)
Wilson B	37.2	36.8	38.7	40.0
Refinement				
No. reflections (work/test)	15170 / 798			
R_{work} / R_{free}	0.213 / 0.264			
No. atoms				
Protein	1127			
Buffer components	8			
Water	77			
B-factors (Å^2)				
Protein	54.5			
Buffer components	71.8			
Water	41.7			
R.m.s deviations				
Bond lengths (Å)	0.018			
Bond angles (°)	1.87			
Ramachandran plot (%)				
Favoured	94.9			
Allowed	2.9			
Outlier	2.2			

The values in parentheses are given for the highest resolution shell. For the native dataset Friedel pairs were merged, for the MAD datasets Friedel pairs were treated as separate reflections.